

K&C Science Report – Phase 2

ALOS-PALSAR Indonesia Forest Monitoring Project

Shaun Quegan, Martin Whittle
CTCD, University of Sheffield, Hicks building, Hounsfield Rd, Sheffield S3 7RH
s.quegan@sheffield.ac.uk, m.whittle@sheffield.ac.uk .

Yumiko Uryu, Koko Yulianto
WWF Indonesia, yumuryu@yahoo.com, kkkyulianto@yahoo.com .

Abstract— Comparison of FBD imagery with deforested areas deduced from land cover maps in the Sumatran province of Riau has shown that both positive and negative changes in HH and HV backscatter can be associated with deforestation. Using the ratios of time separated images a detection rate of 60% at 20% false alarm rate can be achieved. Multi-temporal analysis of ScanSAR time-series for the same region has found that deforestation can best be identified by a relatively high temporal standard deviation. Any attempt to constrain the search to a specific temporal deforestation signature reduces the detection rate. At a false alarm rate of 20% the detection rate is comparable with FBD results, but the data are complementary and can be combined to enhance retrieval to 70%. Large areas of known forest can therefore be rapidly surveyed for evidence of deforestation by measuring temporal variability in a ScanSAR time-series. Further analysis using FBD imagery for suspected areas can refute or support the findings.

Index Terms— ALOS PALSAR, K&C Initiative, change detection, ScanSAR, tropical deforestation

I. INTRODUCTION

A. Phase 2

Tropical deforestation is a major factor in climate change, contributing around 20% of the total amount of anthropogenic carbon dioxide emissions. The 2009 Copenhagen Climate Conference therefore recommended that steps be taken towards establishing the Reduction of Emissions from Deforestation and Degradation (REDD) mechanism [1, 2], which will provide economic incentives for tropical countries to preserve their forests. Yet there is huge uncertainty in the estimates of global deforestation rates [3]. Reducing this uncertainty is crucial to assessments of global carbon balance for climate modeling and harnessing political will for change. Crucial to REDD are reliable methods to monitor tropical forests; these should also, if possible, provide frequent observations so that national authorities can respond quickly to illegal logging. The ScanSAR mode of ALOS-PALSAR seems ideal for this purpose, since it allows wide area

coverage every 46 days and is unaffected by the cloud and smoke that cause serious problems for optical observations in the tropics. Methods to detect deforestation from time-series of ScanSAR images have been developed and applied to the Riau province of central Sumatra. This area is of global significance because much of the forest grows on deep peats, whose degradation after deforestation can lead to major emissions of carbon dioxide. The temporal signature of deforestation is surprisingly varied, and undisturbed forest also shows marked temporal variability, probably caused by changes in soil water. Hence automatic methods achieve high rates of detection of deforestation only at the expense of false detections in undisturbed forest. Visual analysis helps with this problem, but current results suggest that high levels of performance need ScanSAR to be supplemented by less frequent cross-polarized PALSAR data.

B. Scientific findings

Analysis of ScanSAR time series for the Riau and Jambi provinces of Sumatra has shown that deforestation can be associated with both positive and negative changes in HH backscatter. It was not possible to clearly identify any time signatures for the changes that would improve detection characteristics. The implication is that the response associated with deforestation, as deduced from a comparison of the available WWF databases, is very variable. A consequence is that the temporal standard deviation is the best measure to use for detection and using this we have achieved a detection rate of 58% in dry forest and 45% in swampy forest at a false alarm rate of 20%.

Analysis of the backscatter ratios between pairs of FBD images and comparison with WWF databases has shown that positive and negative changes in backscatter can be identified for both the HH and HV channels. Each type can be associated with deforestation deduced from a comparison of WWF land cover databases. A combination of all four types of change leads to an overall deforestation detection rate of 60% at a false alarm rate of 20%. However, in swampy forest the figure is 70% and in dry forest we obtained 47% for our primary sample. This is the reverse of the situation for the

multi-temporal analysis where dry forest gave the better detection rate.

The ScanSAR HH time-series and dual-polarised FBD data contain different information and a fusion of the two types results can lead to an enhancement in the detection rate of up to 10%. At a false-alarm rate of 20% the combination of ScanSAR and FBD results produces an enhanced overall detection rate of ~70%, an improvement over the FBD result of ~10%.

II. PROJECT DESCRIPTION

A. Relevance to the K&C drivers

The key goals of this project are set out in the original proposal as follows:

1. Demonstrate that ALOS ScanSAR and FBD HV data can successfully detect natural forest cover change in Indonesia where cloud and haze hamper natural forest monitoring based on optical remote sensing data.
2. Demonstrate that ALOS data can be used to detect key natural forest and land cover types in Indonesia.
3. Develop software so that ALOS-based monitoring can reasonably easily be done in a scientifically robust manner at technician level.
4. Provide the Indonesian and global community with a tool to transparently, accurately and frequently track natural forest cover change independently of cloud and haze and that can be used as a basis for action on biodiversity conservation, forest carbon management, etc.

Points 1-3 have been addressed – but methods are limited to regions of known forest. We have developed methods using FBD and ScanSAR data and been able to show that both can be competitive with standard optical methods in the tropics provided the forest cover is known as a prior.

B. Work approach

The initial phase of work was directed towards the use of multi-temporal ScanSAR data as a deforestation detection and monitoring tool. Some regions of clearly identifiable deforestation could be identified by a sharp increase followed by decay in backscatter and considerable effort was devoted towards attempting to define signature characteristics as a basis for detection. A comprehensive study of this showed that the changes due to deforestation are very variable and best detected simply by using the temporal standard deviation. A second phase of study has dealt with identification of deforested areas using time-separated FBD images of the same scene. A third area of study has been the combination and mutual support of these two types of data.

C. Satellite and ground data

The work has benefited greatly from access to the WWF 2007 land-cover database for Riau & Jambi [4] and a WWF 2008 database covering a more restricted region partially overlapping the 2007 database. Both are derived manually from Landsat imagery and subject to error partly because of the limited availability of suitable data due to obscuration by cloud. The work described here was restricted to the primary forest area covering the intersection between these databases and a ScanSAR scene, “S1”, and is shown in yellow outline as region “Y” in figure 1. The areas of primary forest indicated as being lost between the years covered by the databases were used as our reference for deforestation.

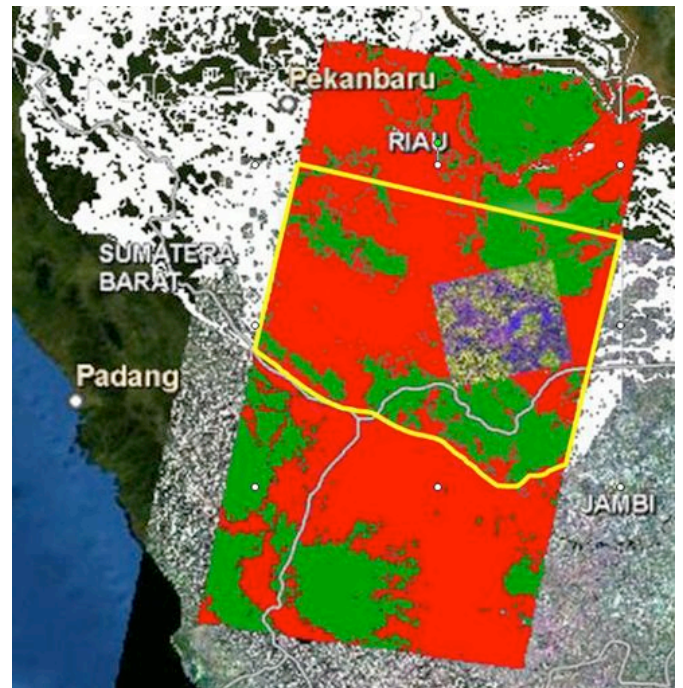


Figure 1. A ScanSAR image of the Riau and Jambi regions of Sumatra overlaid by the WWF 2007 land-cover database, shown with a white outline, and the WWF 2008 database (coloured green to indicate natural forest and red for non-forest areas). The ScanSAR image, S1, is shown as a RGB composite of images acquired in Jan. 2007, Sept. 2007 and June 2008, ALOS K&C © JAXA/METI. The two databases and the ScanSAR footprint intersect in the region “Y” outlined here in yellow. Also shown, fully enclosed by region “Y”, is the FBD scene (path443/frame7170) focussed on in sections 3.3 and 4.2. This is a RGB composite of the HH, HV channels and the ratio HH/HV, ALOS K&C © JAXA/METI. All images are overlaid on a map of the region.

A timeline for the acquisition of these data is shown in figure 2

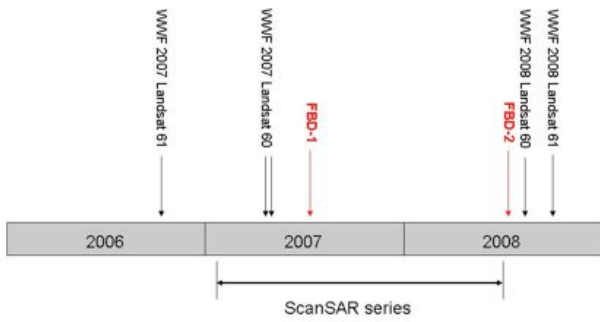


Figure 2 Acquisition timeline for satellite data used in this study. The 12 ScanSAR images were acquired at intervals of 46 days between 2007/01/31 and 2008/06/20. The three FBD images were obtained on 2007/06/28 & 2008/06/30. The WWF databases were derived from Landsat data. For the 2008 database, region “Y” discussed here is covered by images for rows 60 and 61(indicating position in the azimuth direction) acquired on 2008/07/22 and 2008/09/24 respectively. The images used for the same region in the 2007 database were not specified, but suitable Landsat 5 candidates were found for the times indicated on the timeline.

The whole area is subject to very significant monsoon rainfall (200-300 mm / month) between November and March and even between May-September the rainfall is generally more than 100 mm/month. Nevertheless, the 2007 database distinguishes several types of primary forest including “dry” and “swampy” (usually peat swamp) derived from the WWF 2007 database. The region “Y” contains a significant proportion of both types as shown in Figure 3.

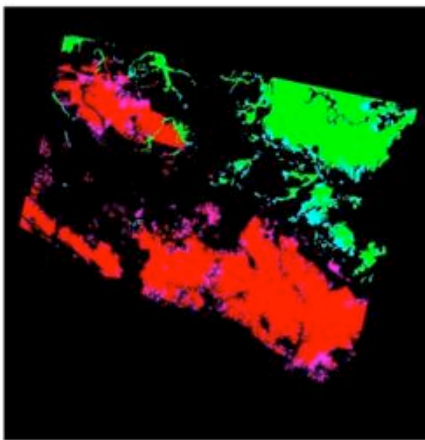


Figure 3 RGB composite showing the areas of primary forest and deforestation derived from the 2007 and 2008 databases in region “Y”. In this image red and green indicate dry and swamp forest respectively. Regions deforested during the interval between construction of the two databases are shown as pink in the dry areas and light blue in the swampy areas.

More recent work to confirm the transferability of our results has extended the study to a second ScanSAR scene, “S2” and two further FBD pairs of time-separated scenes shown in figure 4.

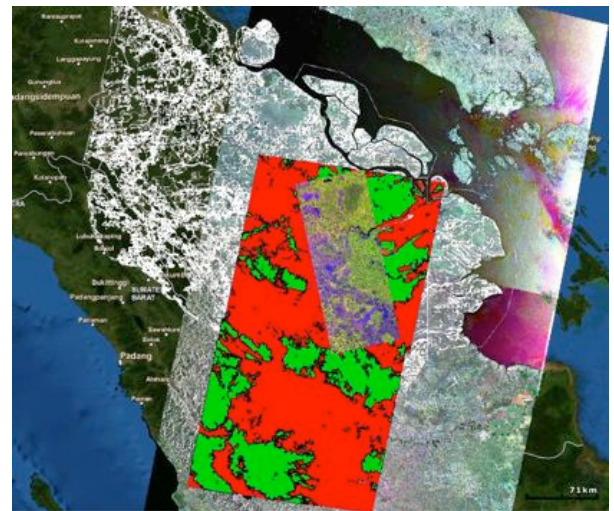


Figure 4. Showing the context of an extended dataset used to study transferability of results. Two ScanSAR composite images (the lower S1 and the upper S2) are overlaid by the WWF 2007 land-cover database, shown with a white outline, and the WWF 2008 database (coloured green to indicate natural forest and red for non-forest areas). The ScanSAR images are RGB composites of images acquired in Jan. 2007, Sept. 2007 and June 2008, ALOS K&C © JAXA/METI. Also shown, are three FBD scenes that also intersect the databases, from the bottom up these have frame numbers 7170, 7180 and 7190 (Table 2). These are RGB composites of the HH, HV channels and the ratio HH/HV, ALOS K&C © JAXA/METI. All images are overlaid on a map of the region.

Table 1 Acquisition dates for ScanSAR scenes used in this work. S1 has path115/frame3650 and S2 path115/frame3600.

No	Date
1	2007/01/31
2	2007/03/18
3	2007/05/03
4	2007/06/18
5	2007/08/03
6	2007/09/18
7	2007/11/03
8	2007/12/19
9	2008/02/03
10	2008/03/20
11	2008/05/05
12	2008/06/20

Table 2 FBD scenes discussed in this work.

No	Path	Frame	Date1	Date2
1	443	7170	2007/06/28	2008/06/30
2	443	7180	2007/06/28	2008/06/30
3	443	7190	2007/06/28	2008/06/30

1) Analyses of ScanSAR Images

Average intensities for both ScanSAR scenes itemized in Table 1 are shown in Figure 5. Images of both scenes were

acquired on the same day (Table 1), so identical image numbers correspond to the same dates in each case. There are differences of up to ~2dB between the average intensities of some images between the two scenes. For scene S1 the highest intensity levels occur in the first and the 8th images dated 31/01/2007 and 19/12/2007 and for scene S2 for the first and the 9th image 03/02/2008. These dates correspond to the seasonal high monsoon rainfall between November and March (> 200mm/month). The lowest levels occur for the 5th the 12th images dated 03/08/2007 and 20/06/2008 corresponding to the “dry” season (75-150mm/month).

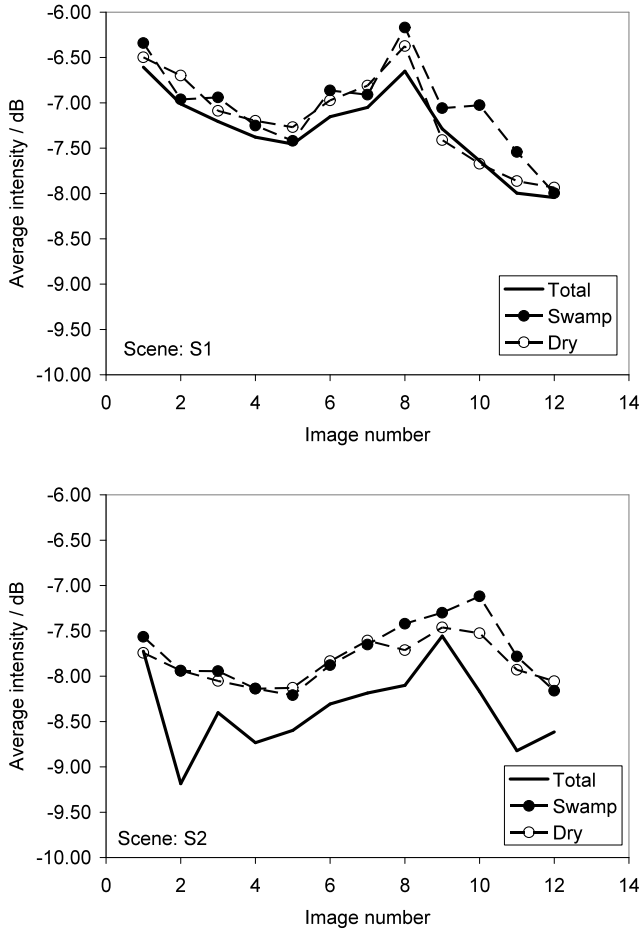


Figure 5 shows the average intensity for scenes S1 and S2 for each of the 12 images. Total refers to the average intensity of the whole image including non-forest areas. Swamp and dry refers to areas designated as swampy and dry in the WWF2007 database.

Since these trends would complicate change detection, they were removed by scaling each image in the series by a factor that makes the mean forest intensity in each image equal to the mean forest intensity for the whole set of images. To achieve this, the mean forest intensity in the k^{th} image, $\bar{I}_f(k)$, is measured, using the forest area given in the 2007 database, and these values are averaged to produce the overall average forest intensity, \bar{I}_f . All pixels in the k^{th} image are then

multiplied by the factor $\bar{I}_f / \bar{I}_f(k)$.

L-band HH measurements in temperate and boreal regions have indicated that forest areas tend to exhibit more stable backscatter than other vegetated or bare soil land cover types [5]. Hence it was expected that general change detection methods would be effective in detecting the presence of deforestation in the ScanSAR time-series, before more detailed analysis locating the event within the series. At each pixel, the change measures considered were:

$$\text{Range: } I_{\max}(\mathbf{x}) - I_{\min}(\mathbf{x}) \quad (1)$$

Standard deviation:

$$SD(\mathbf{x}) = \left[\frac{1}{N-1} \sum_{i=1}^N (I(\mathbf{x}, t_i) - \mu(\mathbf{x}))^2 \right]^{1/2} \quad (2)$$

Mean absolute variation from the mean:

$$AD(\mathbf{x}) = \frac{1}{N} \sum_{i=1}^N |I(\mathbf{x}, t_i) - \mu(\mathbf{x})| \quad (3)$$

Mean absolute inter-image variation:

$$Vm(\mathbf{x}) = \frac{1}{N-1} \sum_{i=1}^{N-1} |I(\mathbf{x}, t_{i+1}) - I(\mathbf{x}, t_i)| \quad (4)$$

Maximum absolute inter-image change:

$$I_{\max c}(\mathbf{x}) = \max_{1 \leq i \leq N-1} [I(\mathbf{x}, t_{i+1}) - I(\mathbf{x}, t_i)] \quad (5)$$

Minimum absolute inter-image change:

$$I_{\min c}(\mathbf{x}) = \min_{1 \leq i \leq N-1} [I(\mathbf{x}, t_{i+1}) - I(\mathbf{x}, t_i)] \quad (6)$$

where $I_{\max}(\mathbf{x})$ and $I_{\min}(\mathbf{x})$ are the maximum and minimum intensity values in the time-series at position \mathbf{x} , and

$\mu(\mathbf{x}) = \frac{1}{N} \sum_{i=1}^N I(\mathbf{x}, t_i)$ is the temporal mean intensity at

position \mathbf{x} , and the images were acquired at times t_i , $i = 1-N$. In addition, at each pixel we measured the net change in intensity from its initial value:

$$\begin{aligned} I_{\text{sum}}(\mathbf{x}) &= \sum_{i=2}^N [I(\mathbf{x}, t_i) - I(\mathbf{x}, t_1)] \\ &= \sum_{i=2}^N I(\mathbf{x}, t_i) - (N-1)I(\mathbf{x}, t_1) \end{aligned} \quad (7)$$

and, for reasons discussed below, we also considered separately those pixels with net positive and negative changes (i.e. those with a net increasing and decreasing trend). Each of these quantities gives rise to two probability density functions (PDFs), and corresponding cumulative frequency distributions (CFDs), one for deforested areas and one for undisturbed forest. Examples of such PDFs and CFDs for the temporal standard deviation measure are shown in Fig. 6; they are calculated over the WWF 2007 forest region within the database intersection area “Y” covering the ScanSAR scene (Figure 1), under the assumption that WWF databases are

accurate.

From the CFDs we can find the proportion of pixels at which any given threshold value is exceeded and hence, for any fixed threshold, the detection probability for true deforestation, P_d , and the false alarm probability for undisturbed forest, P_{fa} .

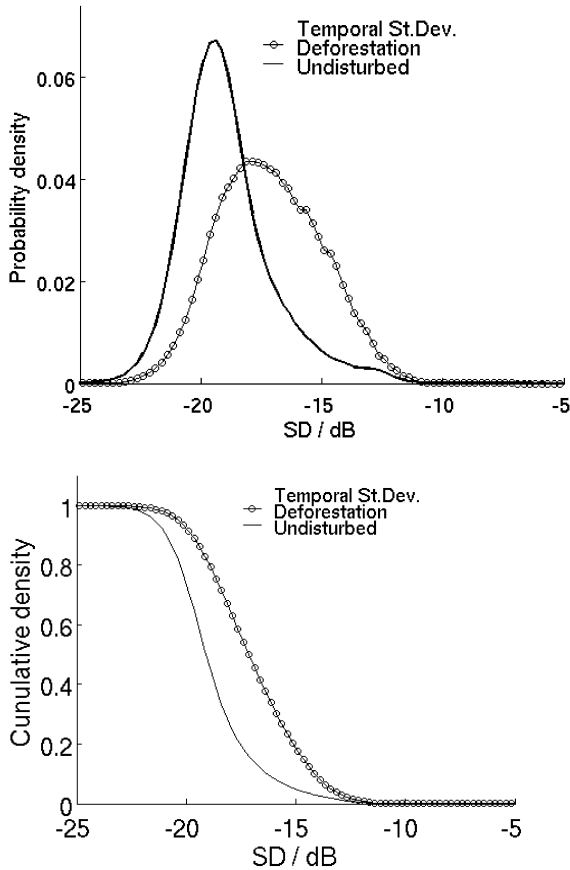


Figure 6 (top) PDFs of the temporal standard deviation in undisturbed forest (—) and deforested (-o-) regions. (bottom) The corresponding CDFs. In this region the undisturbed forest and deforested areas have areas of 827121 and 151380 ha respectively.

The most useful way to display this information is through the “receiver operating characteristic” (ROC) curve, which plots P_d against P_{fa} ; each point on this curve corresponds to a particular threshold value. ROC curves for several change measures are given in Figure 7. In fact the results in Figure 7(a) were obtained by directly counting pixels associated with deforestation and those that are not, for a set of thresholds for each measure. The equivalent result obtained by integrating the PDF for the standard deviation is shown in figure 7(b). The close correspondence between this and figure 7(a) and serves as a check on the methodology. An optimized detection strategy seeks to maximize detections for a given false alarm level, and Fig. 7(a) shows that this is best achieved by the temporal standard deviation (although the range gives almost the same performance), except at unacceptably low

detection probabilities. However, even for a false alarm rate as high as 20%, only ~60% of the deforestation is detected.

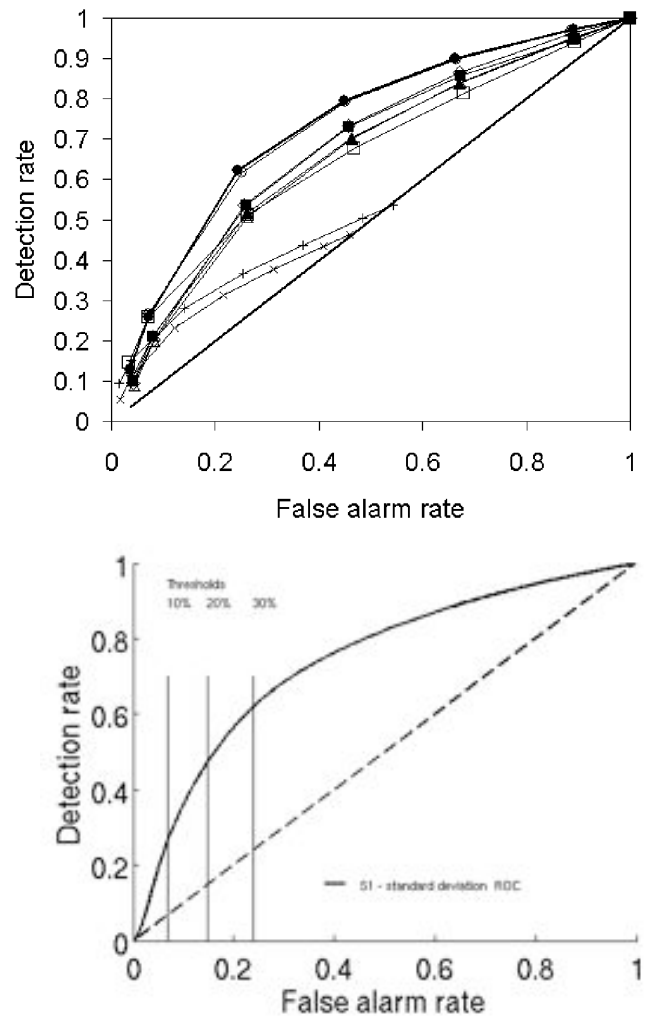


Figure 7. (a) ROC curves for the following change measures over region “Y” obtained by pixel counting: SD —●—; $(I_{max}-I_{min})$ —○—; σ_{max} —■—; V_m —◇—; I_{maxc} —□—; I_{minc} —△—; $|I_{sum}|$ —◆—. The net change in intensity is shown as partial ROC curves: $(I_{sum}>0)$ —+—; $(I_{sum}<0)$ —x—. The solid diagonal line represents the ROC expected if the deforested and undisturbed regions have the same CFD. (b) ROC curve for ScanSAR for region “Y” from integrating the PDF for temporal standard deviation. The top percentile values are shown as vertical lines.

Improved performance would be possible by combining measures if they gave different information. This possibility was tested using Principal Component Analysis of the full set of change measures, but none of the combinations this produced gave results that improved on the standard deviation for discriminating between deforestation and undisturbed forest. Hence this single measure appears to be the most appropriate.

The temporal standard deviation, by definition, is sensitive to all types of variation irrespective of shape. A second method

of improving performance uses a two-stage detection process, the first emphasizing high recall and the second preferentially discarding false alarms to improve the precision of the results, [6]. In our case, using the temporal standard deviation as the primary stage, we tried a number of fitted variables characterising the change as the secondary stage. As well as those described in Eqs(1)-(7), this included variables such as the rise and decay time of a response designed to recognise organized change, which we found to be associated with some regions of deforestation. We found that minor improvements in retrieval were possible at values of false alarm rate below 15% through using the mean absolute inter-image variation Eq(4). This quantity is sensitive to fluctuating variation and less so to more organized change. It possibly produces some enhancement by preferentially screening out fluctuations associated with flooding, for example. However, none of the variables characterizing the shape of the response (peak height, slope, decay rate, etc.) gave any improvement in retrieval by this method. The implication is that the response associated with deforestation as deduced from a comparison of the available WWF databases is very variable and not possible to characterize simply by shape.

Work in tropical and boreal forests has previously suggested that deforestation should lead to a decrease in scattering [7]. However, in some cases, sharp increases in backscatter followed by a relaxation to lower values, were clearly associated with geometrically-shaped regions of deforestation and thus associated with large scale industrial operations. Partial (in that the contributing pixels are mutually exclusive but together cover forest regions used to generate the full curves) ROC curves for the positive and negative net changes in intensity, Eq. 7, are also shown in Figure 7(a). These show that deforestation can be associated with either positive or negative changes in intensity and that positive changes account for slightly more than negative in this scene.

2) Analysis of FBD images

Several Fine Beam Dual images covering part of the forest area covered by database overlap region have also been analysed. The process starts with two FBD intensity images A, B of the same scene acquired at different times. As with the ScanSAR images it has been convenient to concentrate on just the changes that have occurred in the designated forest regions of the WWF2007 database. Thus, non-forest areas are masked out and currently ignored in the analysis. The comparison routine then treats each channel separately. First the two images are normalised to the same average intensity

$$\begin{aligned} A_o(\mathbf{x}) &= \frac{A_f(\mathbf{x})}{\bar{A}_f} * \frac{1}{2} (\bar{A}_f + \bar{B}_f) \quad ; \\ B_o(\mathbf{x}) &= \frac{B_f(\mathbf{x})}{\bar{B}_f} * \frac{1}{2} (\bar{A}_f + \bar{B}_f) \end{aligned} \quad (8)$$

where A_f and B_f are the extracted regions (here forest) in original images A and B and \mathbf{x} denotes pixel position. The results are then processed to give normalised and window-averaged images a and b before ratios are taken.

As an example, we have chosen two images of a single scene acquired a year apart on 28/06/2007 and 30/06/2008 respectively. As shown in figure 1, this scene lies entirely within region “Y” and can thus be compared with ScanSAR results. Regions deforested between the two dates are deduced from differences between the forest regions reported by the two databases. Our initial study used simple ratios $R(\mathbf{x}) = a(\mathbf{x})/b(\mathbf{x})$ of the intensity values, which correspond to differences when viewed on a decibel scale.

As with the ScanSAR analysis above, we found that deforestation could be associated with both “positive” and “negative” changes, where a positive change from $a(\mathbf{x})$ to $b(\mathbf{x})$ means an increase in intensity with time; hence $b(\mathbf{x}) > a(\mathbf{x})$ and $a(\mathbf{x})/b(\mathbf{x}) < 1$ if a is the older image. This occurs for deforestation in both the HH and HV channels. As the window size increases, the width of distributions for $R(\mathbf{x})$ narrows. As defined, “negative” changes have ratio values $a(\mathbf{x})/b(\mathbf{x}) > 0$ and “positive” changes have values $b(\mathbf{x})/a(\mathbf{x}) > 0$. Both types of change can conveniently be combined by defining a quantity R_1 such that,

$$R_1(\mathbf{x}) = \max \left[\frac{a(\mathbf{x})}{b(\mathbf{x})}, \frac{b(\mathbf{x})}{a(\mathbf{x})} \right] - 1, \quad (9)$$

where a “1” is subtracted to adjust the minimum value to zero. The value of R_1 is zero if there is no change and always > 0 for any change “positive” or “negative”. PDF’s for the resulting values are shown in Figure 8.

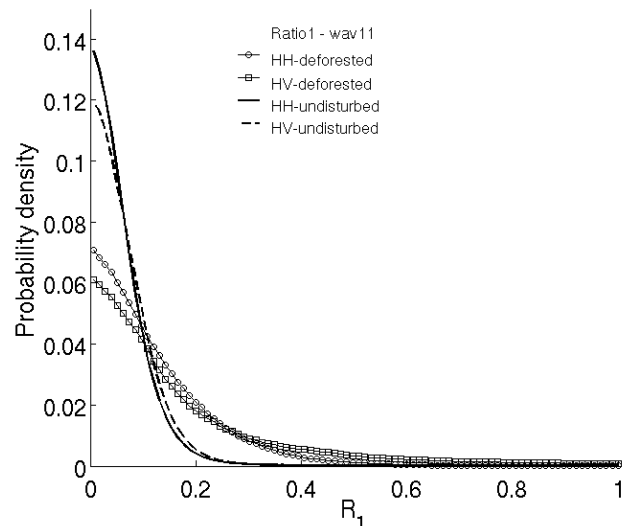


Figure 8 Probability density functions for the value R_1 , HH channel undisturbed () and deforested (\circ -) regions and for the for HV channel undisturbed (- -) and deforested (\square -) regions. Results obtained from window-averaged images using a window size 23×23 .

By integrating the probability density function shown in figure 8 we can obtain detection and false alarm rates for each value of R_1 , and, from these, ROC curves. A number of different methods have been investigated for combining these results but few could compete with the sum of the R_1 values for each channel,

$$R_1^{tot} = R_1^{HH} + R_1^{HV}. \quad (10)$$

Small (<1%) improvements over this method were obtained by combining the HH and HV results using a data fusion technique. This involved ranking the values of both sets of results in ascending order, and then assigning to each pixel the highest rank-value obtained for that pixel by either the HH or HV channels. The linearization of two distributions by this method can improve the chance of a good combination. In this case it seems that the distributions of R_1 values for the HH and HV channels are sufficiently similar to give little advantage in using the more sophisticated method. Beyond this, there is no obvious reason why a simple equal-weighted sum should give the best result and we use the data fusion result, as it perhaps more generally applicable. ROC curves obtained from the R_1 data for the individual HH and HV channels are compared with the best combined result in figure 9.

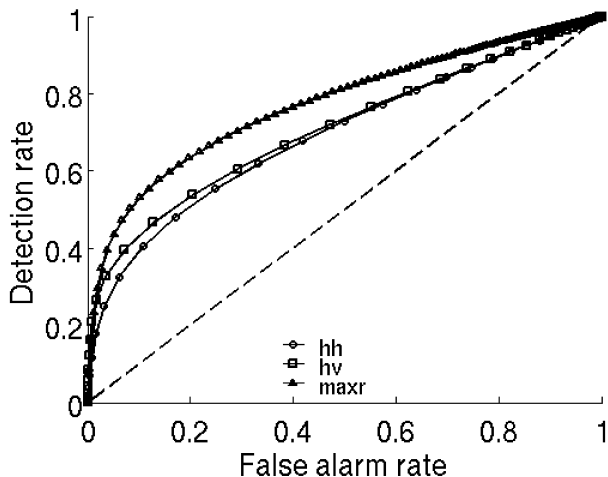


Figure 9. Comparison of HH (\circ -) and HV (\square -) ROC curves obtained from R_1 using a window size 23×23 , and the combined result obtained by maximum-rank data fusion, $maxr$ (Δ -).

Three points are worth noting about this figure. Firstly, the detection capabilities of the HH channel are almost as good as the HV channel: either detects more than 50% of the deforestation at a false alarm rate of 20% as derived from the

WWF databases. Secondly, at this level of false-alarm, the single-channel results are comparable with the ScanSAR multi-temporal detection rate, but much better performance is achieved if only lower false alarm rates can be tolerated. Thirdly, the combined result gives a detection rate of ~65% at a false alarm rate of 20%; i.e. an increase of ~10% over the result for the HV channel alone.

III. RESULTS AND SUMMARY

1) Results for FBD

Figure 10(a) shows the regions selected as having the top combined values of the ratio R_1 for a portion of the FBD scene and are compared directly with the deforested regions picked out in figure 10(b).

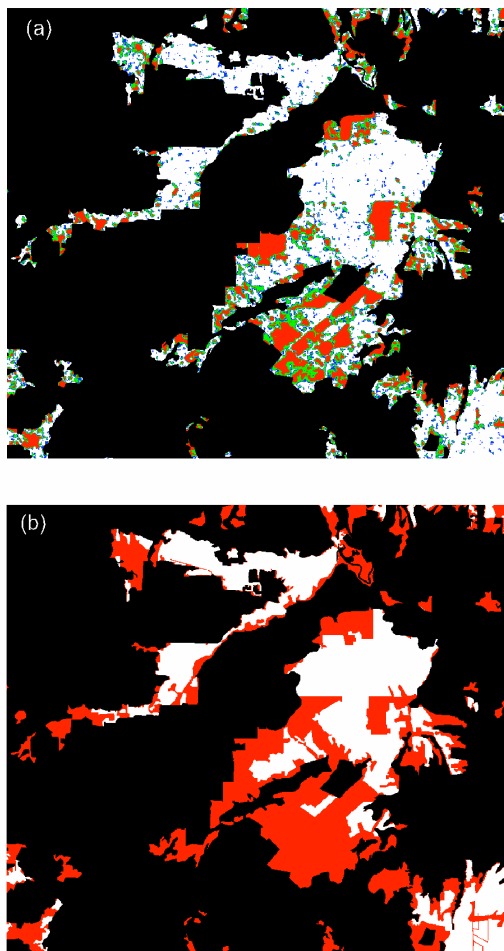


Figure 10 (a) shows pixels from the top percentile values of the combined result from FBD ratio using data fusion for a portion of the scene measuring 40×36 km. All results are for window-averaged images with a window size 23×23 . The ranges are colour coded 10% (red), 10-20% (green), 20-30% (blue) for values of the maximum rank data fusion $maxr$. For comparison, (b) show masks representing the undisturbed forest and deforested areas for the region as derived from the WWF 2007 and 2008 databases.

Figure 11 presents a map of the results over thwhole FBD scene obtained by applying thresholds to select pixels with the highest values of the combined measure. The ROC curve for this measure is included, with the thresholds used superimposed. For this measure a threshold accepting only the top 30% of results retrieves nearly 60% of the deforested regions assigned by the databases for a false alarm rate of 16%. By comparison the top 30% threshold for ScanSAR yields 62% of the deforested regions for a false alarm rate of 23.8% (figure 6)

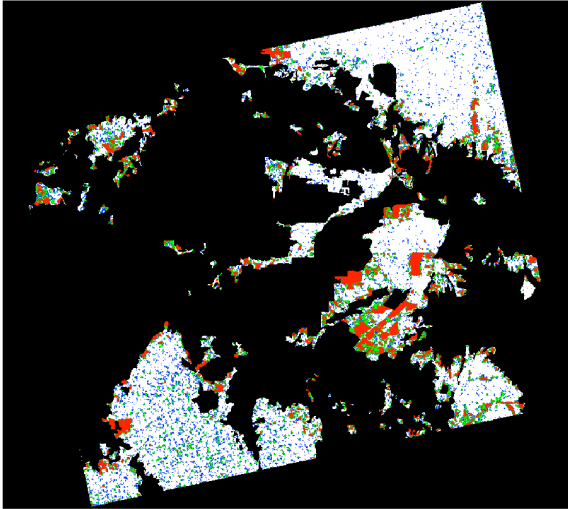


Figure 11. FBD detections for the full scene obtained using R_1 and combining HH and HV channels for the whole FBD footprint (path443/frame7170) measuring 59×70 km. The top percentile ranges are colour coded 10% (red), 10-20% (green), 20-30% (blue) The white area represents the primary forest regions according to the WWF 2007 database.

The combined result for HH & HV FBD is shown, resolved into wet and swampy areas, in Figure 12. It is clear that retrieval in swampy forest is significantly better than in dry for FBD.

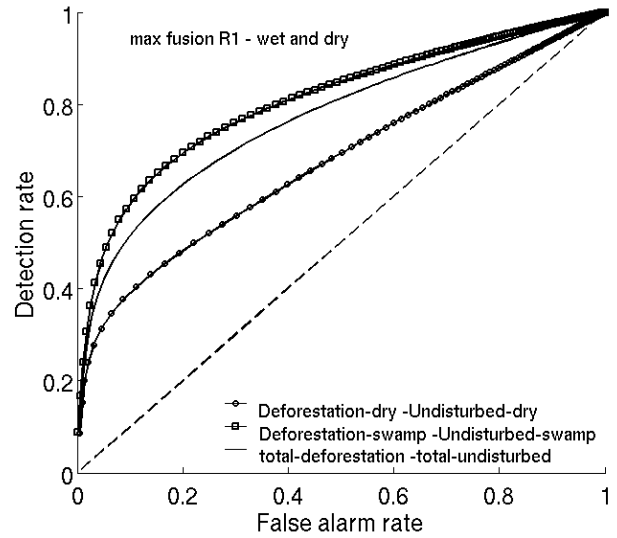


Figure 12 ROC curves obtained using R_1 from window-averaged images using a window size 23×23 followed by data fusion using the maximum-rank technique. For swampy areas (—□—); dry areas (—○—), and both areas (—).

2) Results for ScanSAR

The ROC curves obtained from pdf's of the temporal standard deviation for swampy and dry forest are shown in Figure 13. The combined result for “total” forest is equivalent to that already shown in Figure 7. As for the FBD results, there significant differences between swamp and dry forests, and at the 10% false alarm rate, the probability of detecting deforestation of dry forest is roughly twice that for swampy forest. Thus, while FBD is more sensitive to change in swampy forest, the greater background temporal variability reduces the sensitivity of multi-temporal detection in these regions. The methods are thus complementary.

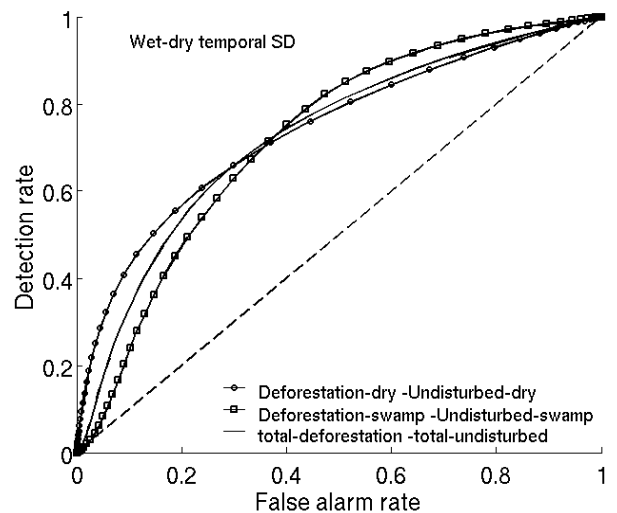


Figure 12 ROC curves for the temporal standard deviation computed for: (—○—) dry, (—□—) swamp, and (—) total forest areas. The dashed diagonal

line shows the expected ROC if the CDFs of undisturbed and forested regions are the same.

A map of the ScanSAR detections over region “Y” obtained from the temporal standard deviation is shown in Figure 14. A detail of this result is shown for the FBD footprint in Figure 15 to allow easier comparison with the FBD detections shown in Figure 11. Many of the areas found to have a high level of change using the FBD images and highlighted in Figure 11 are also represented here. However, there are also significant differences: a large red area left of top centre can be associated with a river valley and the mottled red and green areas to the far right of the image (region “A”) was reached by a WWF ground survey on 18th June 2008 which confirmed that the area is “peat swamp forest of palm, pandan and rattan, with very open canopy, that is frequently flooded”. A different river valley also shows up very clearly at the top left of figure 14 outside the FBD footprint. Colored red it is highlighted as a region of substantial change, but there is very little evidence of any deforestation from the database comparison. The high variability in backscatter associated with flooding in swampy forest is thought to account for the lower detection rate in these regions compared with dry forest (Fig. 13).

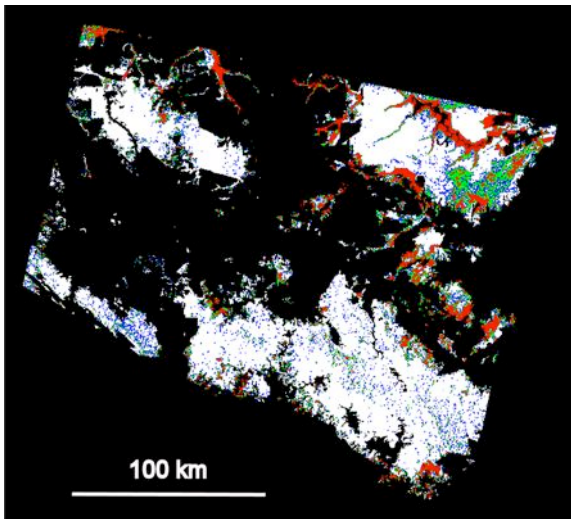


Figure 14. ScanSAR detections for the region Y. Colours correspond to top percentile ranges of the temporal standard deviation 10% (red), 10-20% (green), 20-30% (blue). The white area represents the primary forest regions according to the WWF 2007 database.

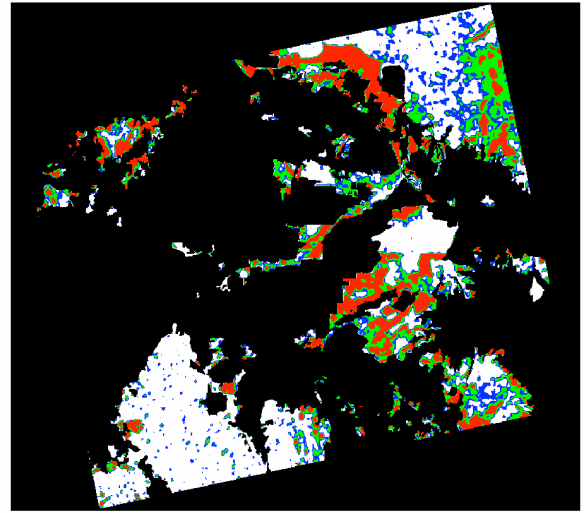


Figure 15. ScanSAR detections for the FBD footprint (59x70 km). Colours correspond to top percentile ranges of the temporal standard deviation 10% (red), 10-20% (green), 20-30% (blue). The white area represents the primary forest regions according to the WWF 2007 database.

3) Combination of FBD with ScanSAR detections

The complementary nature of FBD detection using dual polarisation and multi-temporal single polarisation detection has been demonstrated for the response to dry and swampy forest. It is clear that the methods provide different information and that the complementarity may extend to other factors underlying the detection. It also suggests that a combination of results from the two schemes could be beneficial. Multi-temporal ScanSAR retrieval performance based on the temporal standard deviation is shown in figure 7 for the overlapping region, “Y”, between databases and a single ScanSAR scene. Although this is taken over a different area to the FBD results and hence not directly comparable, it nevertheless suggests that performance is comparatively reduced at low values of the false alarm rate. However, at a false alarm rate of 20% the detection rate of 58% is slightly better than the 55% achieved by the FBD HV channel alone. ScanSAR data is supplied at a different resolution orientation (due to orbital direction) to FBD data, making combination awkward. The procedure adopted here was to obtain rasters of ScanSAR results for the top 10%, next highest 10-20% and next highest 20-30% standard deviations, and convert each to vector graphics, or shape files, using Envi [8]. These were then used to generate three raster masks, which we label SC09, SC08 and SC07 respectively, each with pixel values 0 or 1, covering the footprint of the FBD image. These could be recombined into a single raster, S , with values 0.9, 0.8 and 0.7 using the expression

$$S = 0.7 * SC07 + 0.1 * SC08 + 0.1 * SC09 \quad (11)$$

to represent the three categories. The raster, S , representing ScanSAR detections is composed of pixels co-registered with the FBD results and can now be combined. Because the raster S contains only discrete values and zeros many combination schemes give unsatisfactory results. Our scheme first ranked the combined FBD result followed by re-scaling to give linearised values, \hat{R}_{FBD} , between 0 and 1. These were then combined with the raster S using,

$$R_{combined} = \hat{R}_{FBD} + \left(1 - \hat{R}_{FBD}\right) S. \quad (12)$$

Using this scheme, if a value of \hat{R}_{FBD} is high but S is zero $\hat{R}_{combined}$ retains the high value. If S is non-zero the value of $\hat{R}_{combined}$ is always increased above that of \hat{R}_{FBD} , but because this increase is always mediated by the term $\left(1 - \hat{R}_{FBD}\right)$ the combination has the effect of smoothing the discrete values of S leading to a smooth distribution the combined result. An ROC curve for the combined result is shown in Figure 16 where it is compared with the ROC curve for the best FBD result obtained by combining the HH and HV channels.

At a false-alarm rate of 20% the combination of ScanSAR and FBD produces a detection rate of ~70%, an improvement of the FBD result of ~10%. The result of the fusion is shown as a map for the FBD footprint in figure 17.

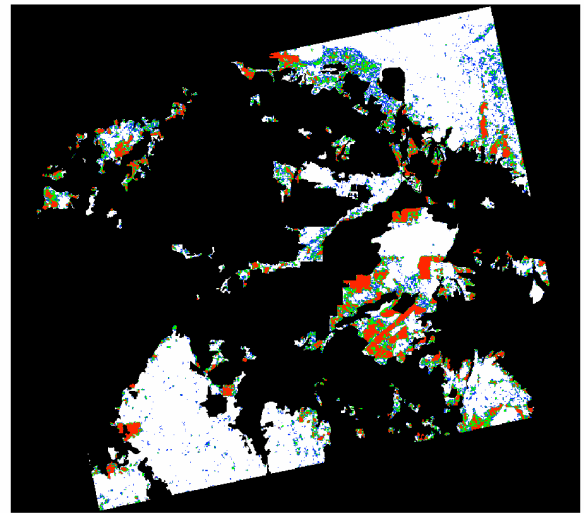


Figure 17 the final result of combining HH,HV and ScanSAR. The percentile ranges are colour coded 10% (red), 10-20% (green), 20-30% (blue) for values of $R_{combined}$. The white area represents the primary forest regions according to the WWF 2007 database.

A comparison of this with best FBD result, figure 11, suggests that the main difference is that the combination has cleaned up some of the noisy areas (e.g. the large area at the bottom left of figure 11) and “moved” the noise to areas where the SCanSAR result disagrees with the FBD result – notably region “A” and the river valley already alluded to above.

4) Transferability

The analysis has, to date, been carried out on one other adjacent ScanSAR scene, S2 in Figure 4, that also covers an intersection of the databases. For this scene the deforestation retrieval rate was reduced to ~46% for a false alarm rate of 20%. The forest cover for this scene is almost exclusively categorized as swampy, and the lower detection rate can be ascribed to the higher temporal variability in this type of forest. Two further FBD scenes (Figure 4) have also been analysed. For one of these (F7180) The detection rate at false alarm rate 20% is 71% for the FBD and slightly improved to 74% for (F7190) combined with ScanSAR; for the other a reduced detection rate of 51% at false alarm rate 20% was obtained and increased to 55% when combined with ScanSAR.

Summary

It is often reported that deforestation should lead to a decrease in scattering for both the HH and HV channels [7]. However, for both the SCanSAR and FBD results we found that positive and negative changes in backscatter intensity can be associated with deforestation. Positive changes can arise if the initial stage of cutting, which reduces attenuation by the canopy, leaves standing trunks which reflect strongly through a double bounce mechanism [9, 10], or a significant amount of

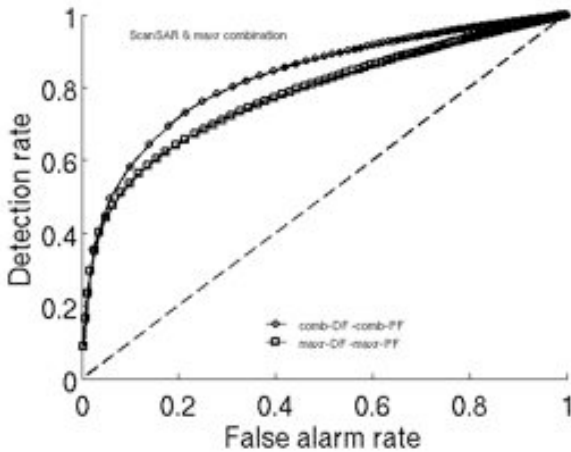


Figure 16 ROC curves for the combined results of HH and HV channels⁵⁾ using the ratio R_1 and widow averaging with window size 23×23 (—□—); further combination with ScanSAR results as discussed (—○—).

branches and other detritus on the ground. In Amazonia, slash and burn methods have been linked to increases in backscatter through the practice of leaving trunks standing and stems and branches on the ground to dry, sometimes for months, before burning and final clearance [11]. Thus the change in backscatter can depend on the stage of deforestation: e.g. slashing, burning and clearing [12]. For the ScanSAR results, we found that some areas of deforestation showed a characteristic temporal signature consisting of an initial rise followed by a relaxation, but the signature was far from universal. This signature is likely to be associated with industrial logging as it appeared for geometrically shaped regions. In general, however, we could find no consistent pattern of change that could be associated with deforestation as defined by the available databases. It is also possible that forest regrowth contributes to some of the changes seen here, as there is some uncertainty in the land cover classification dates, so that deforestation could have occurred before the start of the time-series. Finally, the meaning of deforestation is poorly defined and covers a range of different types of degradation [13]. Other types of deforestation including forest degradation, forest thinning and burning may contribute different signatures depending upon how the databases were constructed.

By using the temporal standard deviation as a general measure of change for a set of ScanSAR images, a detection rate of 58% could be achieved at a false alarm rate of 20% for known primary forest areas. At this level of false alarm rate the method is competitive with a comparison of time-separated FBD images, which achieved a 65% detection rate. A combination of the two types of data is mutually beneficial and raised the detection rate to 73% at this level of false alarm rate. We have also established that comparable results can be obtained for adjacent images.

6) *Future perspective*

The work presented in this report has provided a thorough investigation of the strengths and limitations of ScanSAR and FBD in detecting deforestation in Sumatra. It has shown that conventional wisdom about the primary importance of HV compared with HH is not so clear in this dataset, and that expected indicators of deforestation (reduced HH and HV backscatter) form only part of the measurements need to achieve optimum detection of deforestation. It has also made clear ALOS-PALSAR achieves its best performance when FBD is fused with ScanSAR in the detection process.

ACKNOWLEDGEMENTS

We thank Sue Page, Kevin Tansey and Matt Waldram from the Dept of Geography at Leicester University for helpful discussions. This work has been undertaken within the framework of the JAXA Kyoto & Carbon Initiative. ALOS PALSAR data have been provided by JAXA EORC.

A weakness of the current work is that it has only considered a single (large) region. This leads to two obvious extensions in order to realise the full significance of this work:

1. Apply the same methods other tropical forests, both in Sumatra and in other parts of the tropics, including other parts of Indonesia but also Africa and S. America. Here a key issue is ancillary data to test performance, so ideally this would be done in collaboration with other K & C team members or with other groups able to provide independent deforestation estimates.
2. Evaluate the computing, data and human resources needed to apply these methods over large regions, for example the whole of Sumatra, and investigate the feasibility of doing this.

ALOS-PALSAR should not be seen as the sole sensor suitable for monitoring tropical deforestation, and it needs to be placed within the total global capability relevant to this task. A natural framework for this is provided by the GEO Forest Carbon Tracking initiative: <http://www.geo-fct.org/> and the development of National Forest Monitoring and Carbon Accounting Systems “as part of provision of the technical capability and continuity to support the monitoring, reporting, and verification (MRV) information required by future regulatory frameworks for the inclusion of forests in post-Kyoto climate agreements”. We aim to develop a position for ALOS-PALSAR within these schemes. This was a strong motivation for the work reported here, as we wanted to make sure the use of ALOS-PALSAR was fully understood, so that its use in FCT will be well-founded, use optimal approaches, and have quantified limitations.

We also recognise that, while deforestation is of interest to tropical countries in its own right, its importance is seen internationally in terms of its effects on climate and biodiversity. Hence we would like to interface deforestation observations with ecosystem modelling, along the lines proposed in the GEO-FCT Document 7 “Linking remotely-sensed data, *in situ* forest measurements, and models to calculate GHG fluxes from forests” (Quegan et al., currently only available in draft form, but final form is expected to be completed in February 2011), with the objective of understanding the importance of deforestation in the tropical carbon balance and reducing the very large current uncertainties in GHG fluxes due to land use change.

REFERENCES

- [1] C. Parker, A. Mitchell, M. Trivedi, and N. Mardas, "The Little Redd+ Book," in *An updated guide to governmental and non-governmental proposals for reducing emissions from deforestation and degradation*. Oxford, UK: Global Canopy

- Programme, John Krebs Field Station, Oxford OX2 8QJ, UK, 2008.
- [2] UNFCCC, "Report of the Conference of the Parties on its Thirteenth Session," presented at The United Nations Climate Change Conference, Bali, 2007.
- [3] F. Achard, H. D. Eva, H.-J. Stibig, P. Mayaux, J. Gallego, T. Richards, and J.-P. Malingreau, "Determination of Deforestation Rates of the World's Humid Tropical Forests," *Science*, vol. 297, pp. 999-1002, 2002.
- [4] Y. Uryu, C. Mott, N. Foad, K. Yulianto, A. Budiman, Setiabudi, F. Takakai, Nursamsu, Sunarto, E. Purastuti, N. Fadhli, C. M. B. Hutajulu, J. Jaenicke, R. Hatano, F. Siegert, and M. Stüwe, "Deforestation, Forest Degradation, Biodiversity Loss and CO₂ Emissions in Riau, Sumatra, Indonesia. WWF Indonesia Technical Report," Jakarta, Indonesia 2007.
- [5] S. Quegan, T. LeToan, J. J. Yu, F. Ribbes, and N. Floury, "Multitemporal ERS SAR Analysis Applied to Forest Mapping," *IEEE Transactions on Geoscience and Remote Sensing*, 2000.
- [6] M. Buckland and F. Gey, "The Relationship between Recall and Precision," *Journal of the American Society for Information Science*, vol. 45, pp. 12-19, 1994.
- [7] A. Luckman, J. Baker, T. M. Kuplick, C. C. F. Yanasse, and A. C. Frery, "A Study of the Relationship between Radar Backscatter and Regenerating Tropical Forest Biomass for Spaceborne SAR Instruments," *Remote Sensing of Environment*, vol. 60, pp. 1-13, 1997.
- [8] ENVI, "Image Processing and Analysis: <http://www.itvis.com/ProductServices/ENVI.aspx>," 4.6 ed.
- [9] T. A. Stone and G. M. Woodwell, "Shuttle imaging radar A analysis of land use in Amazonia," *International Journal of Remote Sensing*, vol. 9, pp. 95-105, 1988.
- [10] D. G. Leckie and J. K. Ranson, "Chapter 9 - Forestry Applications Using Imagng Radar," in *Manual of remote sensing. Vol.2, Principles and applications of imaging radar / edited by Floyd M. Henderson and Anthony J. Lewis.*, R. A. Ryerson, Ed., 3rd ed. ed. New York; Chichester: J. Wiley, 1998.
- [11] R. Almeida-Filho, A. Rosenqvist, Y. E. Shimabukuro, and J. R. Santos, "Evaluation and Perspectives of Using Multitemporal L-Band SAR Data to Monitor Deforestation in the Brazilian Amazônia," *IEEE Geoscience and Remote Sensing Letters*, vol. 2, pp. 409-412, 2005.

- [12] R. Almeida-Filho, A. Rosenqvist, Y. E. Shimabukuro, and R. P. Silva, "Detecting deforestation with multitemporal L-band SAR imagery: a case study in Western Brazilian Amazônia," *International Journal of Remote Sensing*, vol. 28, pp. 1383-1390, 2007.
- [13] D. O. Fuller, "Tropical forest monitoring and remote sensing: A new era of transparency in forest governance?" *Singapore Journal of Tropical Geography*, vol. 27, pp. 15-29, 2006.

Biographies



Shaun Quegan received the B.A. (1970) and M.Sc. (1972) degrees in mathematics from the University of Warwick. His Ph.D., awarded by the University of Sheffield in 1982, was concerned with atmospheric modelling. Between 1982 and 1986 he was a Research Scientist at Marconi Research Centre, and led the Remote Sensing Applications Group from 1984-86. He established the SAR Research Group at the University of Sheffield in 1986, whose success led to his Professorship awarded in 1993. In the same year he helped to inaugurate the Sheffield Centre for Earth Observation Science, of which he remains the Director. In 2001 he became the Director of the UK National Environmental Research Council Centre for Terrestrial Carbon Dynamics, which is concerned with assimilating Earth Observation and other data into process models of the land component of the carbon cycle. In addition, since 2008 he has led the Carbon Cycle Theme of the UK National Centre for Earth Observation. He has served on many national and international committees, including the JAXA Kyoto and Carbon Initiative, the ESA Earth Science Advisory Committee (2003-2007) and as Chairman of the Terrestrial Carbon Observations Panel (2002-2007). He was also a co-proposer and member of the Mission Assessment Group for the BIOMASS mission, currently under Phase-A study with ESA. His earlier interests in the physics, systems and data analysis aspects of radar remote sensing are now subsumed in the more general aim of exploiting EO technology to study the Earth's carbon cycle.



Martin Whittle was awarded a B.Sc. degree in Chemistry (1974) and a Ph.D. for work in light scattering (1979) by the University of Manchester. He is a researcher with a background in laser light scattering, infra-red photo-ionisation, particle-based computer simulation of liquids, gels, emulsions, slurries and electro-rheological systems. He has also worked in data mining of web-search databases and virtual screening with a variety of techniques including data fusion in a drug-discovery context.